Figure S1. Sequence alignment of NOP-1 orthologs. NOP-1 orthologs from five Caenorhabditis species were aligned using the Cobolt multiple alignment server (http://www.ncbi.nlm.nih.gov/tools/cobalt/). Ascension numbers are as follows *C. remanei* (XM_003110707.1), *C. briggsae* (XP_002641172), *C. brennerei* (EGT35718; note this sequence contains a pentapeptide, deleted from the alignment that results from a splice donor site that is likely incorrect (GFSI vsdfe KGR), *C. elegans* (CCD68773), *C. japonica* (manually assembled from ABLE01026101).

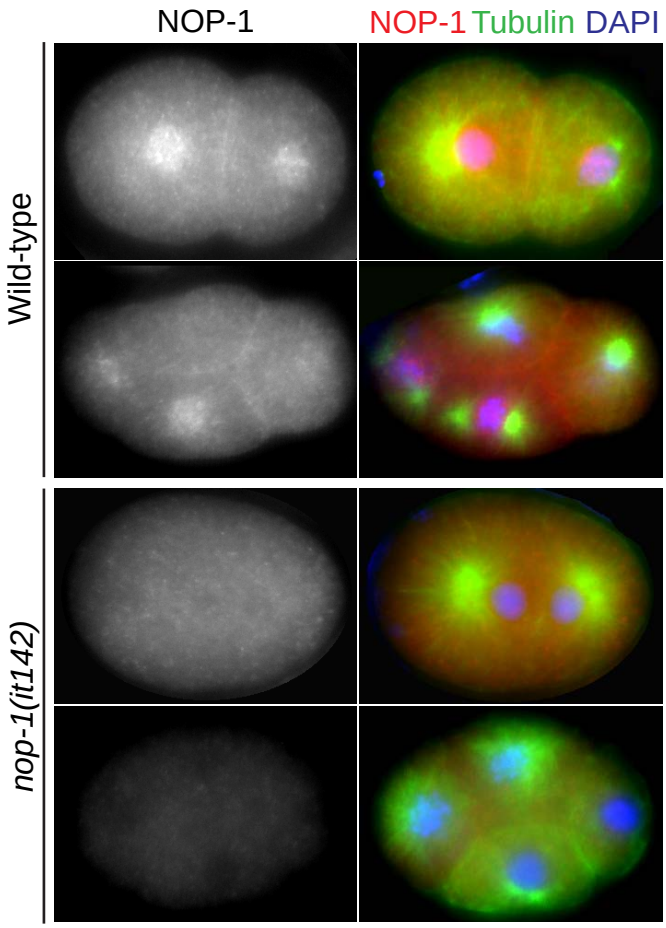

Figure S2. Immunolocalization of NOP-1. Control and *nop-1(it142)* embryos were fixed and immunolabeled with antibodies directed against tubulin and a C-terminal NOP-1 peptide. This epitope is located C-terminal to the premature stop codon in *nop-1(it142)*.

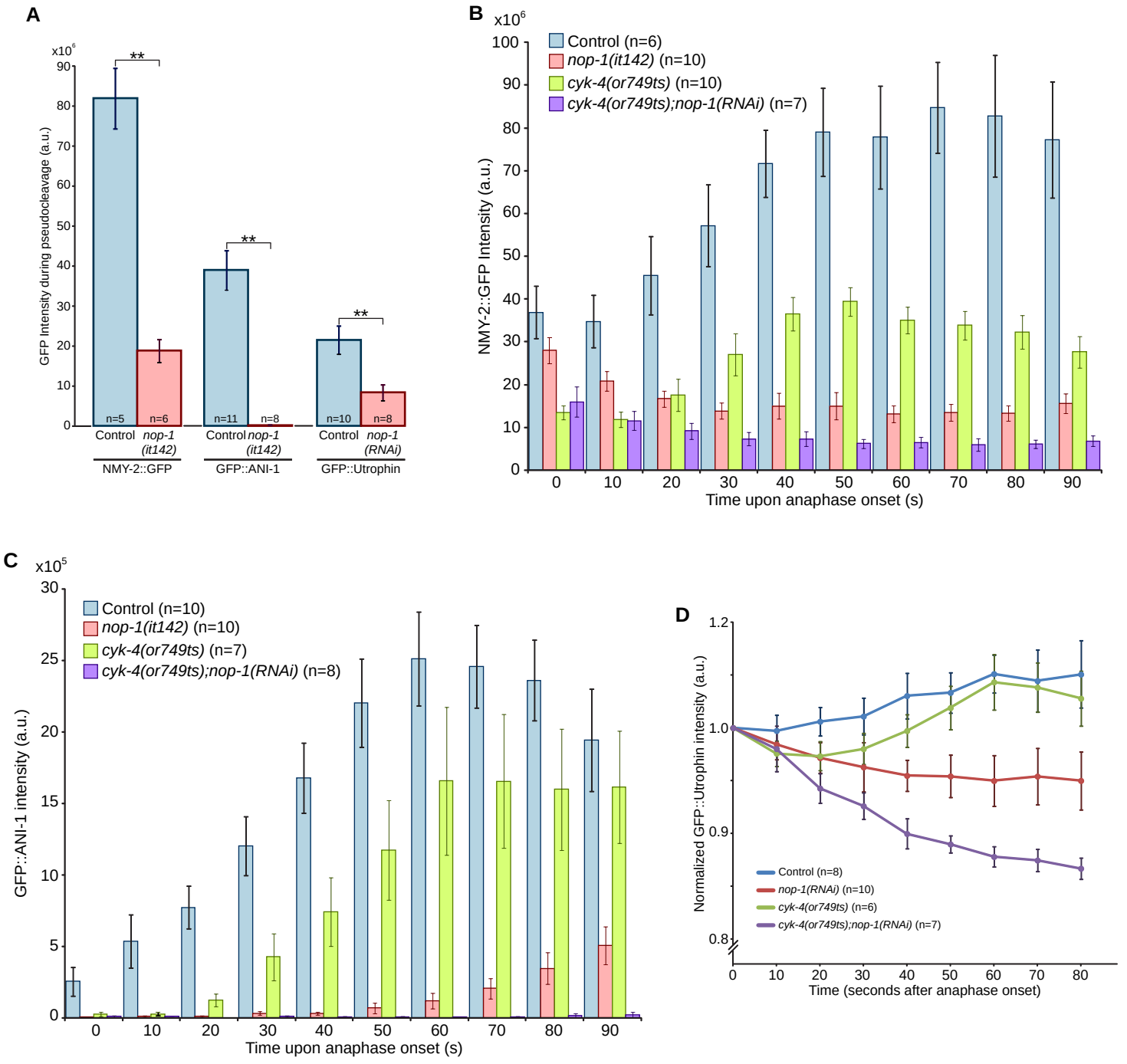

Figure S3. NOP-1 and CYK-4 promote accumulation of RhoA effectors during pseudocleavage and cytokinesis. Images were acquired as described in figures 3 and 4. The accumulation of cortical NMY-2::GFP during pseudocleavage (A) and cytokinesis (B), the accumulation of cortical GFP::ANI-1 during cytokinesis (C), and the accumulation of cortical GFP::Utrophin were quantified as described in the methods section. Error bars represent S.E.M. ** indicates $p < 0.01$.

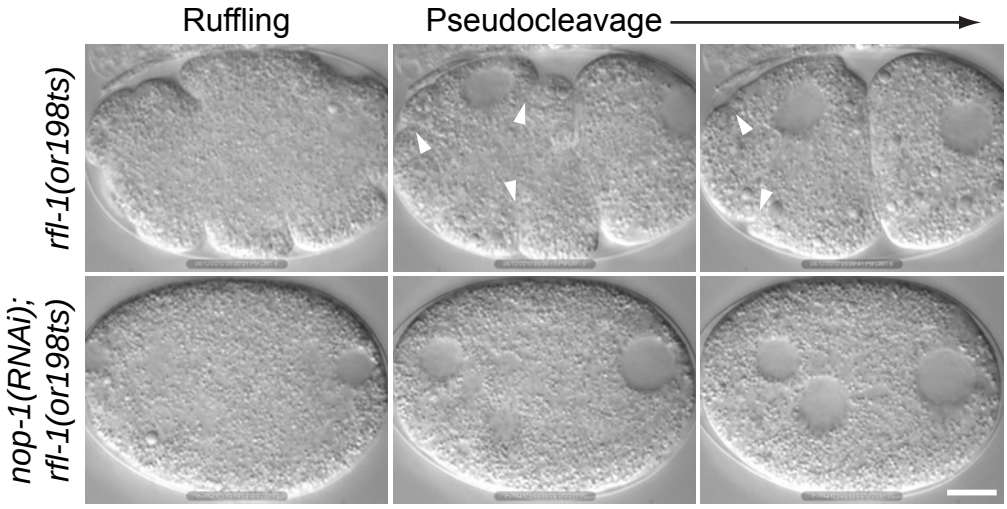

Figure S4. Images from a time-lapse sequences *rfl-1(or198ts)* and, *rfl-1(or198ts);nop-1(RNAi)* embryos during polarization. *rfl-1* embryos are hypercontractile forming ectopic pseudocleavage furrows (white arrows), whereas the contractility is absent in *rfl-1(or198ts);nop-1(RNAi)* embryos. Scale bar represents 10 μm.

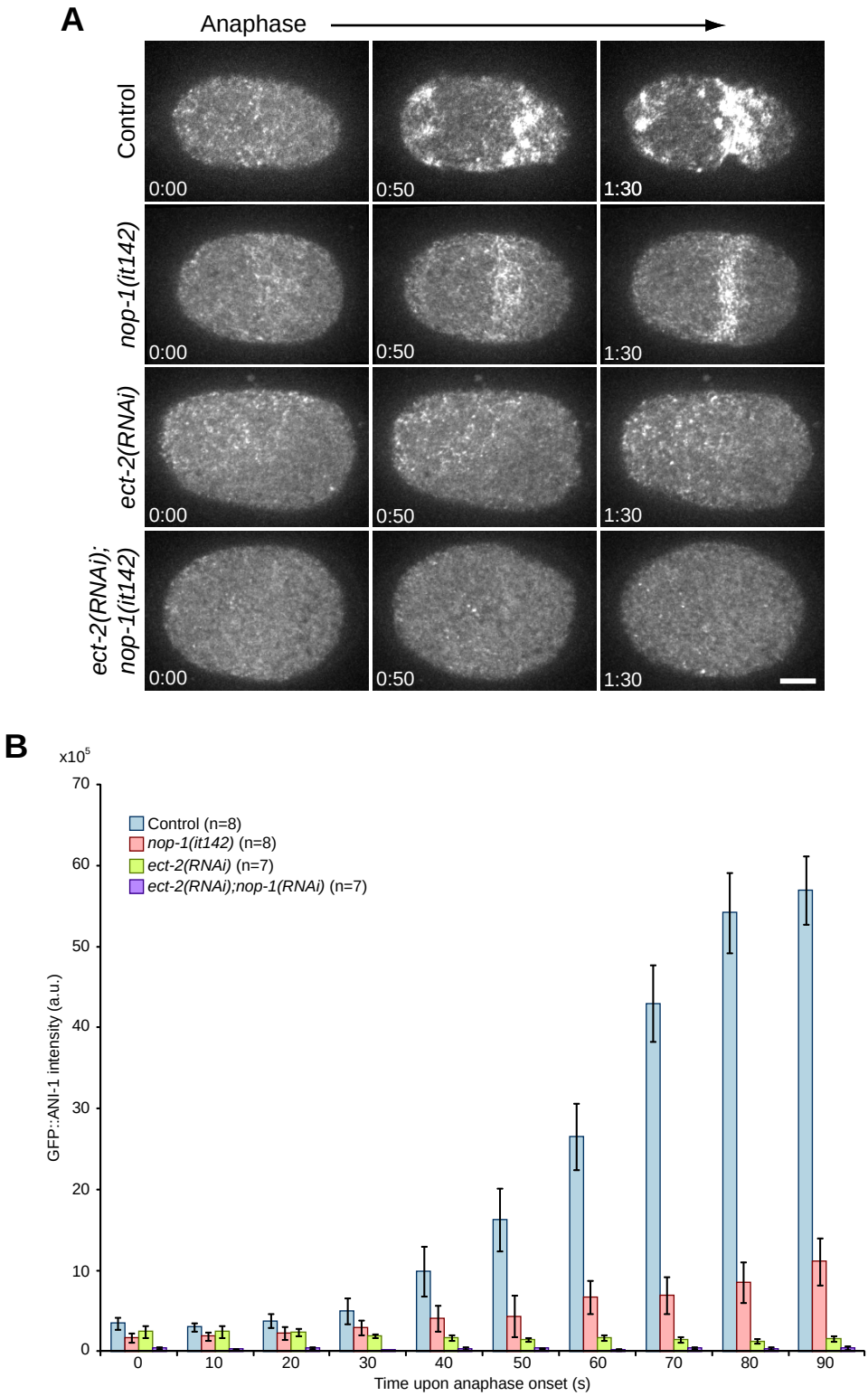

Figure S5. Anillin recruitment is ECT-2 dependent. (A) Cortical confocal images of GFP::Anillin in control, *nop-1(it142), ect-2(RNAi), nop-1(it142);ect-2(RNAi)* embryos at the indicated times after anaphase onset. (B) Quantitation of the accumulation of cortical GFP::ANI-1 from embryos like those in (A). Depletion of ECT-2 all but eliminates recruitment of GFP::ANI-1. Error bars represent ± SEM.

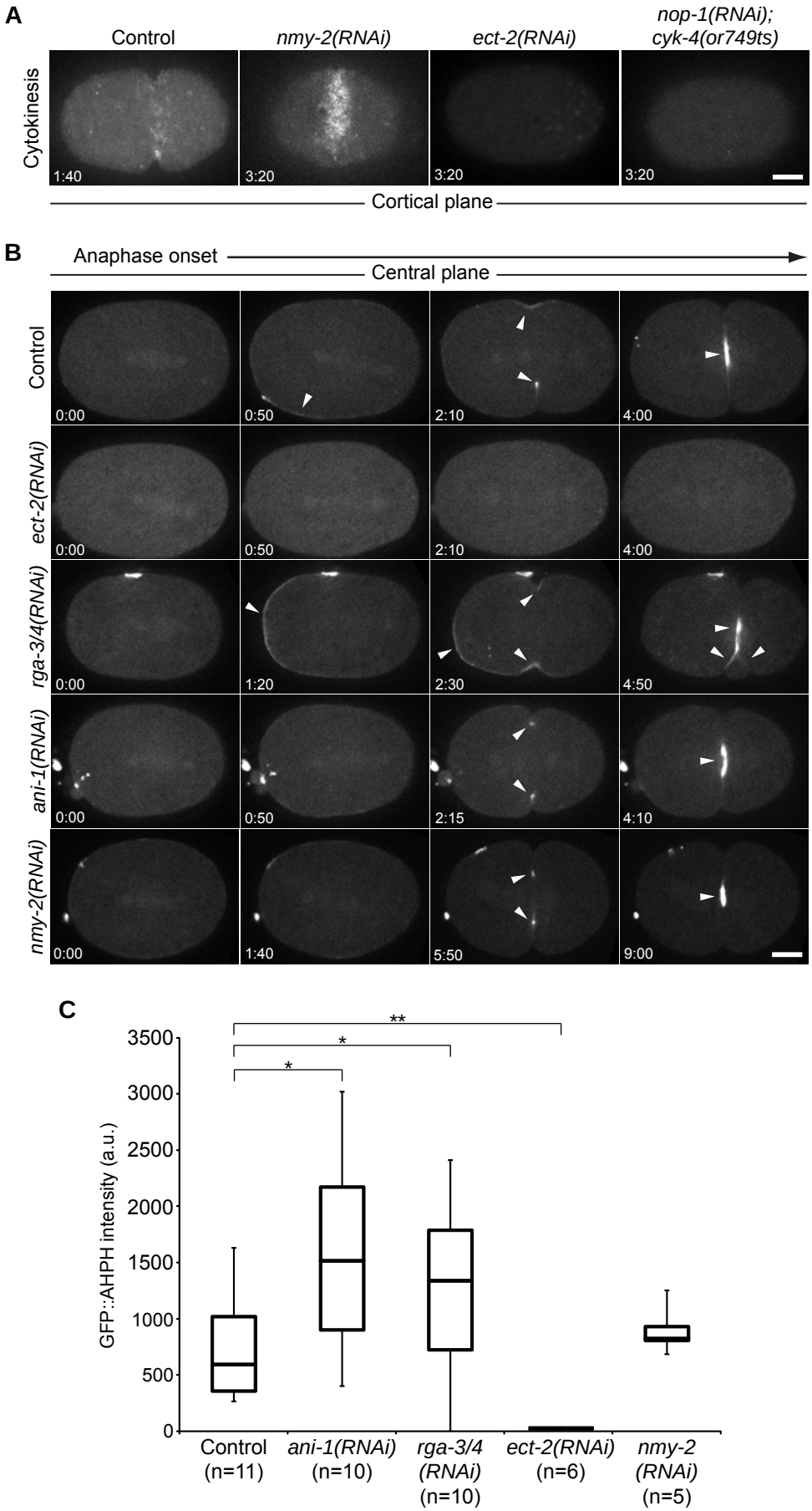

Figure S6. Validation of RhoA reporter. (A) Cortical confocal images of GFP::AHPH in embryos depleted of NMY-2, ECT-2 or *cyk-4(or749ts)* embryos depleted of NOP-1. (B) Accumulation of GFP::AHPH at the midplane of embryos depleted of ECT-2, RGA-3/4, ANI-1, or NMY-2 by RNAi. For the quantitative analysis, we restricted the analysis of NMY-2-depleted embryos to those which furrow to completion, but exhibit pronounced delays in furrowing (~100s). Indicated times represent min:sec following anaphase onset. Scale bar 10 μm. (C) Box-whisker plot of the equatorial accumulation of GFP::AHPH of embryos as shown in (A). ** indicates $p < 0.01$.

Table S1. Worm strains used in this study.

Strain #	Genotype
N2	*Ancestral N2 Bristol strain; "wild-type"*
KK725	*nop-1(it142)*III
MG586	*mgSi2[Cb-UNC-119(+) GFP::NOP-1] II; unc-119(ed3) III*
MG593	*nop-1(it142)III; mgSi2[Cb-UNC-119(+) GFP::NOP-1] II*
MG532	*zuIs45 [nmy-2::NMY-2::GFP + unc-119(+)] V; tjls57 [pie-1::mCherry::HIS-58; unc-119(+)]*
MG576	*nop-1(it142)* III*; zuIs45 [nmy-2::NMY-2::GFP + unc-119(+)] V; tjls57 [pie-1::mCherry::HIS-58; unc-119(+)]*
MG542	*ltIs28 [pASM14; pie-1::GFP-TEV-STag::ani-1; unc-119 (+)]; tjls57 [pie-1::mCherry::HIS-58; unc-119(+)]*
MG567	*nop-1(it142); ltIs28 [pASM14; pie-1::GFP-TEV-STag::ani-1; unc-119 (+)]; tjls57 [pie-1::mCherry::HIS-58; unc-119(+)]*
MG589	*mgSi3[cb-UNC-119 (+) GFP::UTROPHIN]II*
JH2754	*ect-2(ax751) II*
OD239	*cyk-4(or749)III; ltIs38 [pAA1; pie-1/GFP::PH(PLC1delta1) unc-119 (+)]III; ltIs37[pAA64; pie-1::mCHERRY::HIS-58; unc-119 (+)]IV*
MG512	*cyk-4(or749) nop-1(it142)III*
MG520	*cyk-4(or749)III; zuIs45[nmy-2::NMY-2::GFP + unc-119(+)]V; ltIs37[pAA64; pie-1::mCHERRY::HIS-58; unc-119 (+)]*
MG612	*cyk-4(or749)III; ltIs28 [pASM14; pie-1::GFP-TEV-STag::ani-1; unc-119 (+)]; tjls57 [pie-1::mCherry::his-58; unc-119(+)]*
MG628	*cyk-4(or749)III; mgSi3[cb-UNC-119 (+) GFP::UTROPHIN]II; ltIs37[pAA64; pie-1::mCHERRY::HIS-58; unc-119 (+)]IV*
DH244	*zyg-9(b244)II*
MG636	*mgSi5[cb-UNC-119 (+) GFP::ANI-1(AH+PH)]II; nop-1(it142) III*
MG637	*cyk-4(or749)/unc-64(e246)III; mgSi5[cb-UNC-119 (+) GFP::ANI-1(AH+PH)]II; tjls57 [pie-1::mCherry::HIS-58; unc-119(+)]*
MG617	*mgSi5[cb-UNC-119 (+) GFP::ANI-1(AH+PH)]II*
OD58	*unc-119(ed3) III; ltIs38 [pAA1; pie-1::GFP::PH(PLC1delta1); unc-119 (+)]*
MG481	*nop-1(it142)III; ltIs38 [pAA1; pie-1::GFP::PH(PLC1delta1); unc-119 (+)]*
JH2647	*axIs1928 [mCherry::par-6]. oxIs1182 [GFP::par-2]*
JH2657	*ect-2(ax751) II; axIs1928 [mCherry::par-6]. oxIs1182 [GFP::par-2]*
MG596	*nop-1(it142)III; axIs1928 [mCherry::par-6]. oxIs1182 [GFP::par-2]*
EU626	*rfl-1(or198) III.*